Cell Reports

Article

The 3′ UTR of *vigR* is required for virulence in *Staphylococcus aureus* and has expanded through STAR sequence repeat insertions

Graphical abstract

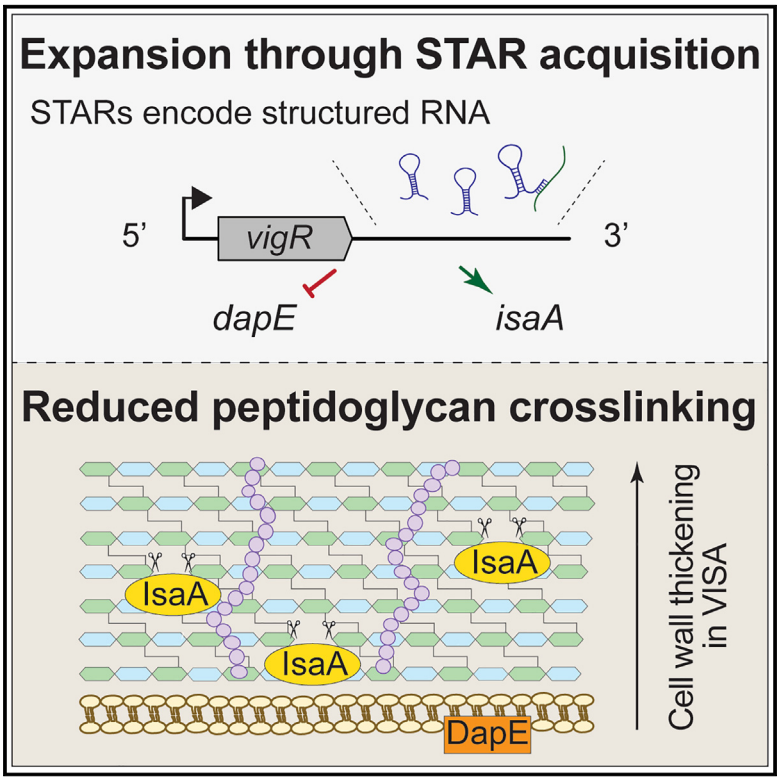

Highlights

- The regulatory *vigR* 3′ UTR is required for pathogenesis in *S. aureus*
- Acquisition of STAR insertions that encode structured RNA has functionalized the 3′ UTR
- *vigR* coordinates a reduction in peptidoglycan crosslinking in a clinical *S. aureus* isolate

Authors

Daniel G. Mediati, William Dan, David Lalaouna, ..., Timothy P. Stinear, Amy K. Cain, Jai J. Tree

Correspondence

daniel.mediati@uts.edu.au (D.G.M.), j.tree@unsw.edu.au (J.J.T.)

In brief

The long 3′ UTR of the *vigR* mRNA contributes to vancomycin tolerance in *S. aureus*. Mediati et al. find that it has expanded through acquisition of structured RNAs termed STARs and is required for virulence. They show that *vigR* regulates *dapE* that contributes to cell wall biogenesis and vancomycin tolerance.

Mediati et al., 2024, Cell Reports *43*, 114082
April 23, 2024
https://doi.org/10.1016/j.celrep.2024.114082

CellPress

Cell Reports

CellPress
OPEN ACCESS

Article

The 3′ UTR of *vigR* is required for virulence in *Staphylococcus aureus* and has expanded through STAR sequence repeat insertions

Daniel G. Mediati,[1,2,*] William Dan,[1] David Lalaouna,[3] Hue Dinh,[4] Alaska Pokhrel,[2,4] Keiran N. Rowell,[5] Katharine A. Michie,[5] Timothy P. Stinear,[6] Amy K. Cain,[4] and Jai J. Tree[1,7,*]

[1]School of Biotechnology and Biomolecular Sciences, University of New South Wales, Sydney, NSW, Australia
[2]Australian Institute for Microbiology and Infection, University of Technology Sydney, Ultimo, NSW, Australia
[3]Université de Strasbourg, CNRS, ARN UPR 9002, Strasbourg, France
[4]School of Natural Sciences, ARC Centre of Excellence in Synthetic Biology, Macquarie University, Sydney, NSW, Australia
[5]Structural Biology Facility, University of New South Wales, Sydney, NSW, Australia
[6]Department of Microbiology and Immunology, Peter Doherty Institute, University of Melbourne, Melbourne, VIC, Australia
[7]Lead contact
*Correspondence: daniel.mediati@uts.edu.au (D.G.M.), j.tree@unsw.edu.au (J.J.T.)
https://doi.org/10.1016/j.celrep.2024.114082

SUMMARY

Infections caused by methicillin-resistant *Staphylococcus aureus* (MRSA) are alarmingly common, and treatment is confined to last-line antibiotics. Vancomycin is the treatment of choice for MRSA bacteremia, and treatment failure is often associated with vancomycin-intermediate *S. aureus* isolates. The regulatory 3′ UTR of the *vigR* mRNA contributes to vancomycin tolerance and upregulates the autolysin IsaA. Using MS2-affinity purification coupled with RNA sequencing, we find that the *vigR* 3′ UTR also regulates *dapE*, a succinyl-diaminopimelate desuccinylase required for lysine and peptidoglycan synthesis, suggesting a broader role in controlling cell wall metabolism and vancomycin tolerance. Deletion of the 3′ UTR increased virulence, while the *isaA* mutant is completely attenuated in a wax moth larvae model. Sequence and structural analyses of *vigR* indicated that the 3′ UTR has expanded through the acquisition of *Staphylococcus aureus* repeat insertions that contribute sequence for the *isaA* interaction seed and may functionalize the 3′ UTR.

INTRODUCTION

Staphylococcus aureus colonizes almost every site in the human body and is increasingly associated with colonization of medical implants.[1] Treatment has been complicated by the emergence of antibiotic-resistant strains, particularly methicillin-resistant *S. aureus* (MRSA) where treatment is limited to last-line antibiotics. The cell wall-targeting glycopeptide antibiotic vancomycin is the treatment of choice for MRSA bacteremia. However, vancomycin treatment failure is increasingly common and attributed to MRSA isolates (up to 13%) with intermediate vancomycin resistance (4–8 μg/mL) termed vancomycin-intermediate *S. aureus* (VISA).[2] VISA isolates have thicker bacterial cell walls that likely limit the permeability of vancomycin to the division septum where binding to cell wall precursors occurs. Single-nucleotide polymorphisms in transcriptional regulators have been reported,[2] suggesting that loss-of-function mutations and changes in gene regulation promote vancomycin tolerance.

Regulatory non-coding RNA (ncRNA) are gene regulators that typically range from 50 to 500 nt and control the expression of target messenger RNA (mRNA) through direct base-pairing. Interactions between ncRNA and mRNA can promote or inhibit degradation by cellular ribonucleases such as RNases that are often associated with the RNA degradosome.[3,4] The canonical pathway of gene regulation involves occluding the ribosomal binding site of a target mRNA leading to translational repression.[5,6] Bacterial regulatory ncRNAs have notable roles in regulating several biological processes including the modulation of the bacterial cell wall (recently reviewed in Mediati et al.[7]), carbon metabolism,[8] and virulence (recently reviewed in Sy et al.[9]). In *S. aureus*, the non-coding small RNA (sRNA) SprD, which is expressed from a pathogenicity island, was shown to repress the immune-evasion protein Sbi and is required for infection in a murine sepsis model.[10] More recently, the sRNA RsaX28 (Ssr42) was implicated in the murine model of skin and soft tissue infection and regulates the expression of multiple virulence factors including the α and γ hemolysins and capsule protein Cap5a through indirect regulation of Rsp[11,12] and through direct interactions with the δ hemolysin and enterotoxin I transcripts (*hld* and *sei*).[13]

The untranslated regions (UTRs) of bacterial mRNAs can act as regulatory elements by base-pairing with target mRNAs, affecting translation and transcript stability. In our previous

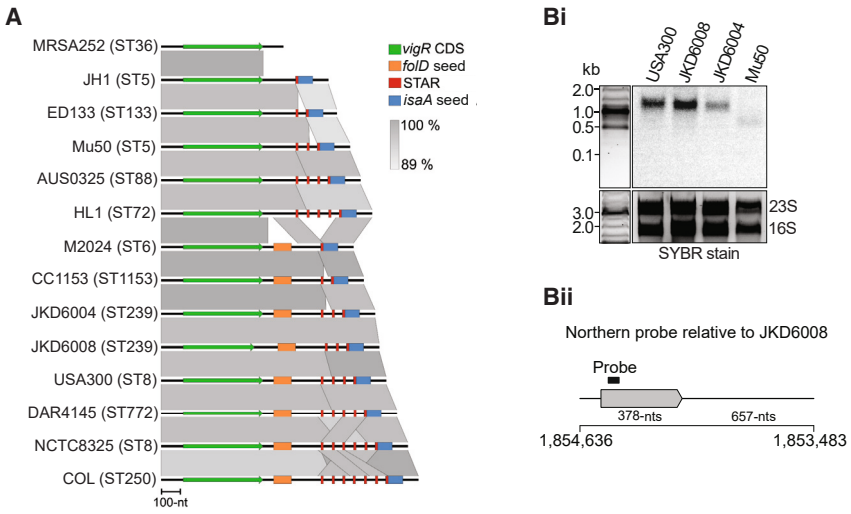

Figure 1. The *vigR* 3′ UTR varies in length between *S. aureus* isolates

(A) Genomic alignment of the *vigR* transcript within 14 representative *S. aureus* strains extracted from dRNA-seq and Term-seq analyses. The VigR coding sequence (CDS) is represented in green, and sequence expansion elements are indicated for the *folD* mRNA interaction seed (orange), *isaA* mRNA interaction seed (blue), and STAR insertional elements (red) (right) within the 3′ UTR. The degree of sequence conservation is indicated (right).

(Bi) Northern blot analysis of the *vigR* transcript. Total RNA was purified from *S. aureus* isolates indicated (top) and probed for the *vigR* CDS. SYBR Green-stained 23S and 16S ribosomal RNAs are indicated below as loading controls. (Bii) Schematic diagram of the Northern blot probe relative to the *vigR* mRNA in *S. aureus* strain JKD6008. The nucleotide genomic position and length of the CDS and 3′ UTR are indicated (below) representative of the *vigR* transcription start site (+1 site).

work, we demonstrated that the unusually long 3′ UTR of the *vigR* mRNA partly mediates vancomycin tolerance by upregulation of the cell wall lytic transglycosylase IsaA.[14] Some 3′ UTRs of mRNAs have been found to expand through insertion of sequence repeats, including *Alu* elements in eukaryotes[15] and IS elements in bacteria.[16] In *S. aureus*, the genome contains *Staphylococcus aureus* repeats (STARs) that are short, repetitive motifs often separated by spacer sequences.[17] While the distribution of STARs varies between closely related staphylococci species, *S. aureus* isolates of the same evolutionary lineage (i.e., same multi-locus sequence type) maintain a similar arrangement of STARs.[18] The STAR sequences have been linked to pathogenesis[18]; however, their function, acquisition, and mechanism of propagation all remain unclear.

We have recently profiled the *in vivo* RNA interactome associated with the double-stranded endoribonuclease RNase III and mapped these interactions to genomic elements in the clinical MRSA isolate JKD6009.[13,14] Surprisingly, we found that the *vigR* 3′ UTR functions as a regulatory mRNA "hub" required for glycopeptide tolerance.[14] In this study, we have used MS2-affinity purification coupled with RNA sequencing (MAPS) to provide a more focused snapshot of the RNA interaction partners of the *vigR* 3′ UTR. We find that *vigR* 3′ UTR interacts with mRNAs involved in carbon metabolism, amino acid biogenesis, cell wall biogenesis, and virulence. We confirm a direct mRNA-mRNA interaction for the target *dapE*, a succinyl-diaminopimelate desuccinylase required for L-lysine and cell wall peptidoglycan precursors. With our earlier finding that the *vigR* 3′ UTR upregulates IsaA,[14] our data here suggests that *vigR* may play a broader role in controlling cell wall biogenesis in *S. aureus*. Deletion of the *vigR* 3′ UTR ($vigR^{\Delta 3'UTR}$) significantly increased the virulence of VISA in a wax moth larvae model of pathogenesis, and we find that an *isaA* deletion is completely attenuated. Sequence analyses of *vigR* from a cross-section of *S. aureus* sequence types indicated that the 3′ UTR is highly variable and has expanded through the acquisition of STAR sequence repeat insertions. We propose that expansion of the 3′ UTR may create a binding site for ribonucleases or RNA-binding proteins that functionalize the UTR in *S. aureus*.

RESULTS

The long 3′ UTR of *vigR* has expanded through STAR insertions

In our earlier work, we demonstrated that the 3′ UTR of *vigR* contributes to vancomycin tolerance.[14] To understand if the *vigR* 3′ UTR is broadly conserved in *S. aureus* isolates, we examined sequence variation within the *vigR* mRNA across 58 *S. aureus* genomes that represented a cross-section of sequence types and clonal complexes. The 5′ and 3′ transcript boundaries of *vigR* were previously defined in our differential RNA-sequencing (dRNA-seq) and Term-seq analyses[14] and were used to extract *vigR* mRNA sequences with 5′ and 3′ UTRs. Both the 5′ UTR and coding sequence (CDS) of *vigR* are highly conserved between the 58 *S. aureus* genomes and did not vary in length, except for the CDS in strains JKD6008 and JKD6009 (378 nt cf. 423 nt) (Figure 1A). In these isogenic strains, a SNP has introduced a premature stop codon that truncates the VigR protein by 15 amino acids. VigR is a hypothetical protein, and it is unclear if the truncated VigR is functional; however, these results suggest that *vigR* may be a pseudogene in the JKD6008/9 pair and may partly explain why we did not observe an antibiotic sensitivity phenotype for the $vigR^{\Delta CDS}$ strain.[14]

In contrast, the length of the *vigR* 3′ UTR varied from 102 to 819 nt across *S. aureus* genomes (Table S1). To confirm that the *vigR* 3′ UTR varied between *S. aureus* isolates, we performed Northern blot analysis on RNA extracted from strains USA300 (mRNA = 1,191 nt), JKD6008 (mRNA = 1,154 nt), JKD6004 (mRNA = 1,131 nt), and Mu50 (mRNA = 999 nt) (Figures 1B and S1). In these strains, we verified that the *vigR* mRNA transcript varied in length consistent with the variation predicted within the 3′ UTR from our sequence analysis (Figure 1A).

We next examined the *vigR* 3′ UTR to identify sequences that were responsible for the expansion. Alignment and visualization of 14 *vigR* mRNA sequences that represent the diversity of 3′

UTR lengths indicated that expansion had occurred in two regions. The first region encompasses 162 nt at genomic position 1,850,825–1,850,986 nt (using strain COL as a reference) (compare strains HL1 and M2023, insertion indicated in orange, Figure 1A). This site has introduced a mRNA interaction seed region with complementarity to the target *folD* mRNA.[14] The second region spans genomic position 1,850,277–1,850,705 nt (in strain COL) and contains the predicted seed for the target mRNA *isaA* (indicated in blue, Figure 1A). This region also contains a repeated sequence that has expanded between *S. aureus* isolates (red, Figure 1A). Examination of the repeated sequences indicated the presence of a previously described STAR sequence repeat element with the consensus 5' – TNTGTTGNGGCCCN.[17] Among the genomes analyzed, the *vigR* 3′ UTR contained 0–7 STAR insertions separated by ~40 nt "spacer" sequences (Table S1).

The spacer sequences between consecutive STARs are reported to be poorly conserved compared to the STAR motif.[18] To better characterize the spacer-STAR sequences in *S. aureus* strain JKD6008, we used GLAM2 and GLAM2SCAN[19] to identify 101 spacer-STAR repeats throughout the entire JKD6008 genome and assembled a consensus sequence motif (Figure 2A and Table S2). In line with previous studies, we find that the STAR motif is well conserved, and our analysis extends the 5′ end of the STAR consensus sequence by 4 nt to 5′ – TCTNTGTTGNGGCCCN – 3′. In addition, we find that the 12 nt at the 5′ end of the spacer is also well conserved among the 101 spacer-STAR sequences (Figure 2A).

Spacer-STAR sequences contain a conserved RNA structure

Given the expansion of spacer-STAR repeats in the *vigR* 3′ UTR, we next asked if spacer-STAR loci are transcribed in other genomic contexts. Spacer-STAR sequences were mapped to the *S. aureus* transcriptome, and we found that 24 were within 3′ UTRs, 10 within 5′ UTRs, and 17 within predicted sRNAs (defined by SRD[20]) (Figure S2A). The remaining 50/101 were within intergenic regions but not within our experimentally defined transcriptome boundaries.[14] These results indicate that many spacer-STAR sequences are inserted into UTRs and sRNAs, suggesting that spacer-STAR sequences may encode a functional RNA.

To determine if spacer-STAR inserts encode conserved RNA structure, we first used CMFinder[21] to identify co-varying nucleotides indicative of conserved structure within our 101 spacer-STAR sequences in *S. aureus* JKD6008. Consensus RNA structures and sequences were analyzed for statistically significant covariation using R-scape[22] and visualized using R2R.[23] We identified 5 statistically significant co-varying bases positioned within a single stem-loop of the spacer-STAR insertion (Figure 2B and Table S3). This conserved RNA stem-loop structure is positioned from +960 to 980 nt of the *vigR* 3′ UTR in our GLAM2 motif (Figure 2A) and corresponds to the poorly conserved spacer sequence. These data indicate that while there is low sequence conservation in the spacer, an 8 base-pair-long RNA stem-loop structure is conserved. While not statistically significant (likely due to high sequence conservation), the conserved 5′ spacer and 3′ STAR sequences are predicted to form an RNA duplex at the base of the structure (Figure 2B). To further validate these structural findings, we used the deep-learning prediction software RoseTTAFold2NA (RF2NA)[24] to predict the backbone structures for the 3 spacer-STAR sequences of *vigR* 3′ UTR (Figure 2C). Consistent with our CMFinder analysis (Figure 2B), RF2NA predicted RNA stem-loop structures for all 3 spacer-STAR sequences (Figure 2C).

Collectively, these data indicate that the *vigR* 3′ UTR has expanded within *S. aureus* genomes through insertion of a 162-nt sequence and spacer-STAR repeats. While the sequence of the STARs and 5′ end of the spacer are conserved, positions +960–980 nt of the spacer encode an 8 base-pair-long RNA stem-loop with variable sequence suggesting that the RNA structure—rather than the sequence—of the spacer is functionally important.

Spacer-STAR repeats are structured *in vitro*

To confirm that the spacer-STAR sequence forms a conserved RNA structure, we used benzyl cyanide and lead acetate to probe the *in vitro* secondary structure of the *vigR* 3′ UTR from *S. aureus* JKD6008 (Figures 2D and S2B). Local nucleotide reactivity and flexibility were analyzed using RNAstructure[25] to predict secondary structure within the *vigR* 3′ UTR. We find that the 3′ UTR is highly structured and that the third spacer-STAR repeat (STAR 3) forms the stem-loop structure predicted by sequence covariation (Figure 2B) and RF2NA, albeit with base-pairing between the STAR motif of repeat 2 and 3, rather than the conserved 5′ motif and STAR 3 (shaded blue in Figure 2D). The spacer-stem of STAR 2 is partially retained (+906–919, Figure 2B) but appears to have been lost from STAR 1 in our structure prediction. Overall, our *in vitro* structure probing data of *vigR* 3′ UTR support formation of at least one spacer-STAR stem-loop structure predicted by sequence covariation.

vigR 3′ UTR represses the *dapE* mRNA

The 3′ UTR of *vigR* was shown to interact with the *folD* and *isaA* mRNAs,[14] where the latter encodes a lytic transglycosylase that cleaves the β-1,4-glycosidic bonding between the *N*-acetylmuramic acid (MurNAc)-*N*-acetylglucosamine (GlcNAc) residues of cell wall peptidoglycan. While deletion of *isaA* reduced cell wall thickness and conferred sensitivity to the glycopeptide antibiotic teicoplanin, the *isaA* mutation does not confer the same vancomycin sensitivity seen in the *vigR* 3′ UTR deletion,[14] suggesting that *vigR* may have additional targets in VISA strain JKD6008. Previous work determined that the *vigR* 3′ UTR functions as a regulatory mRNA (without independent transcription or processing).[14] To identify interaction partners for the *vigR* 3′ UTR we used MAPS.[26,27] The MS2 RNA aptamer was fused to the 5′ end of the *vigR* 3′ UTR and placed under the control of the $P_{xyl/tet}$ promoter of pRAB11.[28] Inducible transcription of MS2-*vigR* 3′ UTR was confirmed by Northern blot, and we found that 15 min of induction with anhydrotetracycline (ATc) led to strong accumulation of the MS2 fusion (Figure S3). The MS2 fusion was induced in JKD6009 grown in brain heart infusion (BHI) medium to an OD_{600nm} 3.0 (mid-log growth phase). Cells were pelleted and lysed before loading onto an amylose column loaded with MS2 protein-His-MBP fusion to pull down the MS2 aptamer. After washing, bound RNAs were eluted with maltose

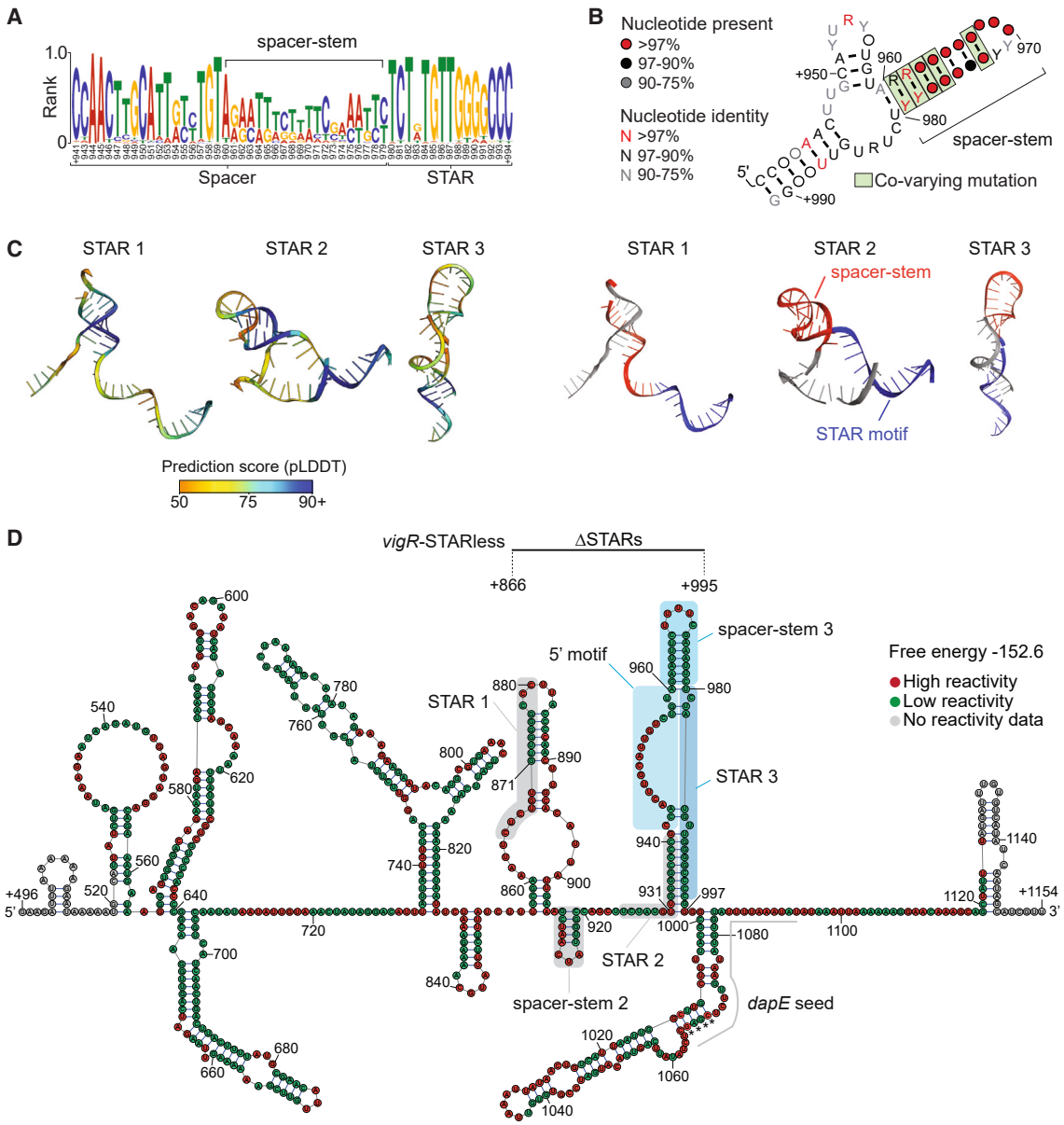

Figure 2. Spacer-STAR sequence repeats encode a conserved RNA structure

(A) Consensus sequence motif of 101 spacer-STAR repeats identified within VISA isolate JKD6008 determined using GLAM2. The numbering of positions in the motifs are based on the numbering of spacer-STAR 3 of *vigR* (see D).

(B) Consensus RNA structural motif of spacer-STAR repeats using CMFinder identifies co-varying nucleotides. Statistically significant covariation (green) was determined using R-scape. The numbering of positions in the motif is based on the numbering of spacer-STAR 3 of *vigR* (see D). Probability of nucleotide presence and identities are indicated (left).

(C) RF2NA predicted RNA structures of the Spacer-STARs within *vigR*. Cartoon rendering with ribbon backbone is colored according to the predicted local distance test (pLDDT) accuracy metric (left). The average pLDDTs were 0.71, 0.72, and 0.67 for STARs 1, 2, and 3, respectively (right). Cartoon rendering of each STAR indicates the spacer-stem (red) and STAR motif (blue).

(D) The *in vitro* secondary structure of the *vigR* 3′ UTR from JKD6008. Benzyl cyanide and lead acetate were used to modify the RNA backbone, and nucleotide reactivity (right) was determined by separation on TBE-urea gels. The nucleotide positions are relative to the transcription start site of *vigR*. STAR motifs 1 and 2 are indicted by gray boxes. Spacer-STAR repeat 3 is indicated by blue boxes. Each section (5′ motif, spacer-stem, and STAR motif) is indicated for spacer-STAR 3. The nucleotides predicted to interact with the *dapE* mRNA are indicated by the gray line. Asterisks indicate the positions where the *isaA* and *dapE* interaction sites overlap.

and precipitated for library preparation and sequencing.[26,29] Peaks were called within the sequencing datasets using blockbuster[30] and CRAC software.[31] DESeq2[32] was used to identify 81 statistically significant peaks enriched in the duplicate MS2-*vigR* 3′ UTR samples compared to MS2-only controls ($p < 0.01$) (Table S4). Clusters of orthologous group (COG) analyses for statistically significant transcripts enriched in MS2-*vigR* 3′ UTR MAPS indicated that functional classifications associated with "Carbohydrate transport and metabolism," "Amino acid transport and metabolism," and "Cell wall, membrane and envelope biogenesis" were enriched (adjusted $p < 0.05$, Figure 3A). To identify interactions that affect the abundance of target RNAs, we correlated our MAPS enrichment data with differential expression data from the *vigR* 3′ UTR deletion (*vigR*$^{\Delta 3'UTR}$) strain.[14] A total of 22 mRNA transcripts were enriched >2-fold by MAPS and had >2-fold increased expression in *vigR*$^{\Delta 3'UTR}$ (Figure 3B, red dotted line), suggesting that *vigR* 3′ UTR may repress these mRNAs through a direct RNA-RNA interaction.

We used electrophoretic mobility shift assays (EMSAs) to verify a direct RNA-RNA interaction *in vitro*. The mRNAs *dapE*, *spn*, and *hysA* that represented different levels of enrichment by MAPS and RNA-seq were *in vitro* transcribed from JKD6008 and incubated with radiolabeled *vigR* 3′ UTR before separation on native 4% TBE PAGE gels. Only the *dapE* mRNA (SAA6008_RS11085) was gel shifted by *vigR* 3′ UTR, and we find that the complex formed between these long RNAs (657 nt and 1,295 nt, respectively) did not migrate out of the well (Figure 4A, EMSA for *spn* and *hysA* mRNAs in Figure S4A). To identify the interaction site, we divided the *dapE* mRNA into 3 subfragments and repeated the EMSA (Figure S4B). The *vigR* 3′ UTR was able to gel shift *dapE* Frag-B (462 nt) encompassing genomic position 2,162,029–2,162,473 nt (Figures 4B and S4C). To further narrow down the interaction site, antisense competitor oligonucleotides (termed 1–4) were tiled across the interaction site between Frag-B and *vigR* 3′ UTR (Figures 4C and 4D). The 31-nt antisense oligo 4 was able to compete away *dapE* Frag-B from *vigR* 3′ UTR (Figure 4C). This site contains a predicted 28 base pair interaction between *dapE* and *vigR* 3′ UTR, with 22 nt of complementarity (Figure 4E). Notably, the *dapE* seed sequence (+1,066–1,094 nt) partially overlaps the *isaA* mRNA seed region at +984–1,069 (Figure 2D).[14] These data suggest that this region within the *vigR* 3′ UTR can base pair with multiple mRNA targets.

To verify that the interaction between *vigR* 3′ UTR and *dapE* mRNA is functional, we expressed *vigR* from the constitutive P_{tufA} promoter of the pICS3 vector[33] and assessed *dapE* mRNA abundance using RT-qPCR (Figure 4F). Consistent with our earlier RNA-seq analyses, we find that *dapE* is 6.1-fold repressed by *vigR* ($p = 0.0026$, $n = 4$, Figure 4F). We confirmed this result using Northern blotting analyses that showed the abundance of *dapE* was increased in *vigR*$^{\Delta 3'UTR}$ and restored in the 3′ UTR chromosomal repair strain (chromosomal knockin, *vigR*$^{\Delta 3'UTR::\ \Delta 3'UTR}$) (Figure S4D). Northern blotting analyses was used to determine the role of the endoribonuclease RNase III in the regulation of the *dapE* mRNA (Figure 4G). These data confirmed a 2.71-fold increase in abundance of the *dapE* transcript in the absence of RNase III (Δ*rnc*) relative to the isogenic parent strain, consistent with *dapE* forming an RNA substrate for RNase III processing.

Collectively, these data indicate that *vigR* 3′ UTR represses *dapE* through a direct base pair interaction with the CDS of the mRNA. DapE encodes succinyl-diaminopimelate desuccinylase that is required for L-lysine and peptidoglycan synthesis,[34] and our results indicate that in addition to activation of the cell wall lytic transglycoslase *isaA*, *vigR* represses *dapE* that contributes to cell wall biosynthesis.

Deletion of the *dapE* mRNA confers increased vancomycin tolerance in VISA

vigR is a regulatory mRNA that controls a glycopeptide-specific intermediate resistance in VISA.[14] To determine the impact of the target *dapE* on intermediate vancomycin resistance, a *dapE* mRNA deletion (Δ*dapE*) was constructed in VISA JKD6008, and an agar spot dilution assay was used to assess vancomycin sensitivity. In the absence of vancomycin, the Δ*dapE* strain had comparable growth to the isogenic parent strain and vancomycin-sensitive *S. aureus* (VSSA) JKD6009 (Figure 4Hi). However, in the presence of a sub-inhibitory concentration of vancomycin (3 μg/mL), growth of JKD6008 Δ*dapE* was increased 1000-fold when compared to wild type (Figure 4Hii). We have also confirmed the vancomycin sensitivity reported for JKD6009 (Figure 4H).

Given that *vigR* interacts to negatively regulate *dapE* in *S. aureus* (Figures 4A–4F), we next asked if constitutive expression of the *vigR* mRNA from the pICS3 vector (pICS3*vigR*) could mimic the increased vancomycin tolerance phenotype observed in Δ*dapE*. The pICS3 constructs were also subjected to an agar spot dilution assay to assess vancomycin sensitivity (Figure S5A). In the absence of vancomycin, all pICS3 constructs had comparable growth, yet in the presence of sub-inhibitory concentrations of vancomycin, growth of pICS3*vigR* was increased 10-fold when compared to the pICS3 empty vector. A truncation of *vigR* that does not contain the native STAR sequences but retains the target *dapE* seed sequence was also cloned into pICS3 and transformed into the Δ*vigR* background (pICS3*vigR*-STARless, Figure 2D). The pICS3*vigR*-STARless construct was not able to increase vancomycin resistance, indicating that the STARs are required for vancomycin tolerance (Figure S5A).

These results demonstrate that deletion of *dapE* confers increased intermediate vancomycin resistance and that *vigR* contributes to vancomycin tolerance in VISA partly through repression of the *dapE* mRNA.

The *vigR* 3′ UTR controls vancomycin tolerance and virulence in a wax moth larvae model of infection

Intermediate vancomycin resistance in *S. aureus* isolates have been correlated with a decrease in virulence in both murine bacteremia and wax moth larvae models of infection.[35,36] We next asked if the decreased vancomycin tolerance of our *vigR*$^{\Delta 3'UTR}$ strain also results in increased virulence in a wax moth larvae model. We infected larvae ($n = 20$) with 10 μL of 10^7 CFU/mL of VISA JKD6008 (isogenic parent), the *vigR*$^{\Delta 3'UTR}$ strain, and chromosomal rescue strain *vigR*$^{\Delta 3'UTR}$-repair (*vigR*$^{\Delta 3'UTR::\Delta 3'UTR}$) where the wild-type 3′ UTR genotype has been restored.[14] We also included the VSSA strain JKD6009

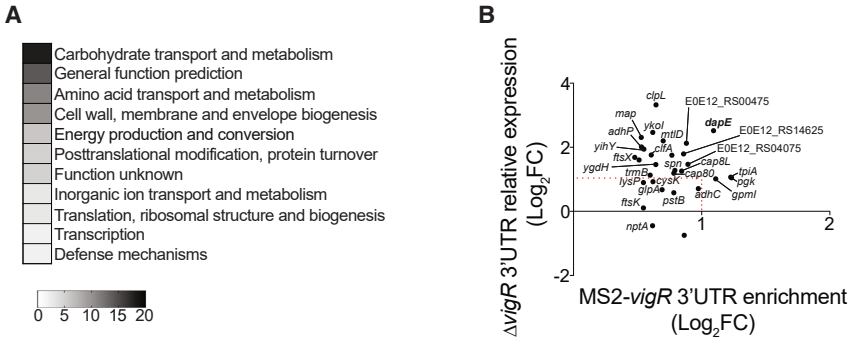

Figure 3. MAPS identifies the extended regulon of *vigR* 3′ UTR in *S. aureus*

(A) Clusters of orthologous groups (COGs) detailed for the 81 statistically significant enriched transcripts found in duplicate MS2-*vigR* 3′ UTR MAPS experiments (adjusted $p < 0.05$). The most abundant COGs are listed in numerical order.

(B) Correlation of enriched transcripts from MAPS (bottom) with dysregulated transcripts from RNA-seq of JKD6008 $vigR^{\Delta 3'UTR}$ (left).[14] The red dotted line indicates those transcripts with a $\log_2FC \geq 1$ in both MAPS and RNA-seq datasets.

that is the parent strain of JKD6008.[2] Infected larvae were monitored for 6 days for melanization and death. Consistent with earlier studies,[35,36] we find that JKD6009 is significantly more virulent than the VISA derivative JKD6008 ($p = 0.0001$, Figure 5A). Deletion of the *vigR* 3′ UTR significantly increased the virulence of JKD6008 ($p = 0.031$), and wild-type virulence was restored in the $vigR^{\Delta 3'UTR}$-repaired strain (Figure 5A). This result indicates that the 3′ UTR of *vigR* contributes to both the reduced virulence and vancomycin-intermediate resistance of VISA strain JKD6008.

To understand whether *vigR* 3′ UTR and *dapE* contribute to vancomycin tolerance during infection, we treated larvae with 10 mg/kg of vancomycin directly after injection with JKD6009, JKD6008, $vigR^{\Delta 3'UTR}$, and Δ*dapE* strains (Figure 5B). Consistent with *in vitro* results, treatment with vancomycin did not significantly affect the virulence of VISA JKD6008. However, vancomycin treatment significantly reduced killing in the $vigR^{\Delta 3'UTR}$ strain and reduced virulence to wild-type levels ($p = 0.022$, Figure 5B). The addition of 10 mg/kg of vancomycin delayed complete killing of larvae infected with VSSA JKD6009 by 1 day (Figure S5B) and did not significantly alter pathogenesis of Δ*dapE* (Figure S5C). These results indicate that the regulatory 3′ UTR of *vigR* is required for intermediate vancomycin resistance in VISA during infection.

We had previously shown that the 3′ UTR of *vigR* upregulates the cell wall lytic transglycosylase *isaA* that contributes to cell wall thickening in VISA JKD6008.[14] We additionally infected larvae with the JKD6008 Δ*isaA* strain to determine if *vigR* 3′ UTR regulation of *isaA* contributes to the virulence phenotype. In contrast to the *vigR* 3′ UTR, deletion of *isaA* completely attenuated JKD6008 ($p = 0.0036$, Figure 5A). Our results demonstrate that while deletion of *isaA* reduces cell wall thickness comparable to the virulent VSSA JKD6009,[14] virulence is not restored to VSSA levels in the VISA Δ*isaA* background. Our data indicate that the cell wall lytic transglycosylase IsaA plays a critical role in *S. aureus* infection.

DISCUSSION

In earlier work, the regulatory 3′ UTR of *vigR* was found to control vancomycin tolerance and upregulate the lytic transglycosylase *isaA*.[14] Using MAPS, we demonstrate that the *vigR* 3′ UTR also represses *dapE* that is required for L-lysine and peptidoglycan synthesis.[37] Our results suggest that the *vigR* 3′ UTR may play a broader role in controlling cell wall metabolism in *S. aureus*, and we demonstrate that the *vigR* 3′ UTR also contributes to the attenuated virulence of the vancomycin-intermediate isolate. Surprisingly, we find that *isaA* is not required for growth *in vitro*, but the Δ*isaA* strain is completely attenuated in a wax moth larvae model of pathogenesis.

Sequence analysis of *vigR* indicated that the 5′ UTR and CDS are highly conserved. In contrast, the 3′ UTR is highly variable and appears to expand through the acquisition of STAR sequence repeat insertions.[17] Here, we have extended the reported 14-nt STAR sequence to include a conserved 5′ TCTN and we find that while the ~40 nt variable spacers do not have conserved sequence, they form an evolutionary conserved RNA stem-loop structure suggesting that the structure of the spacer region is functional. Our *in vitro* structure probing data support the formation of an RNA stem in the spacer region.

It is not yet clear how the spacer-STAR elements influence the function of the *vigR* 3′ UTR, but it is notable that repeat elements have previously been linked to mRNA stability in bacteria and eukaryotes.[16,38–43] Sequence repeats termed SINE elements (notably *Alu* elements in humans) are known to modulate RNA-RNA and RNA-protein interactions when inserted into eukaryotic 3′ UTRs.[38,43] *Alu* elements in 3′ UTRs are reported to provide interaction sites for the dsRNA ribonuclease Staufen.[44,45] In a mechanism that may functionally parallel our observations with *vigR*, 3′ UTR-encoded *Alu* repeats facilitate interactions with *Alu*-encoding long non-coding RNAs (lncRNAs).[44] Imperfect base-pairing of the 3′ UTR and lncRNA recruits Staufen, triggering Staufen-mediated decay and repression of the mRNA target. The *isaA*-interacting nucleotides (seed region) in *vigR* partially overlaps STAR 3 of *vigR*, indicating that this interaction is partly driven by acquisition of the STAR sequence repeat insertion. By analogy, the imperfect base-pairing between the *vigR* STAR sequences and mRNA targets may create a binding site for ribonucleases or recruit RNA-binding proteins.

In our previous work, we postulated that the *vigR* 3′ UTR interactions with *isaA* and *folD* mRNAs may occlude an RNase cleavage site to stabilize the transcripts.[14] This is in line with previous work showing that the regulatory mRNA-mRNA interactions between *hyl-prsA* and *irvA-gbpC* stabilize their targets by occluding interactions with RNase J1.[46,47] Here, we find that *vigR* represses *dapE*, suggesting a mechanism where

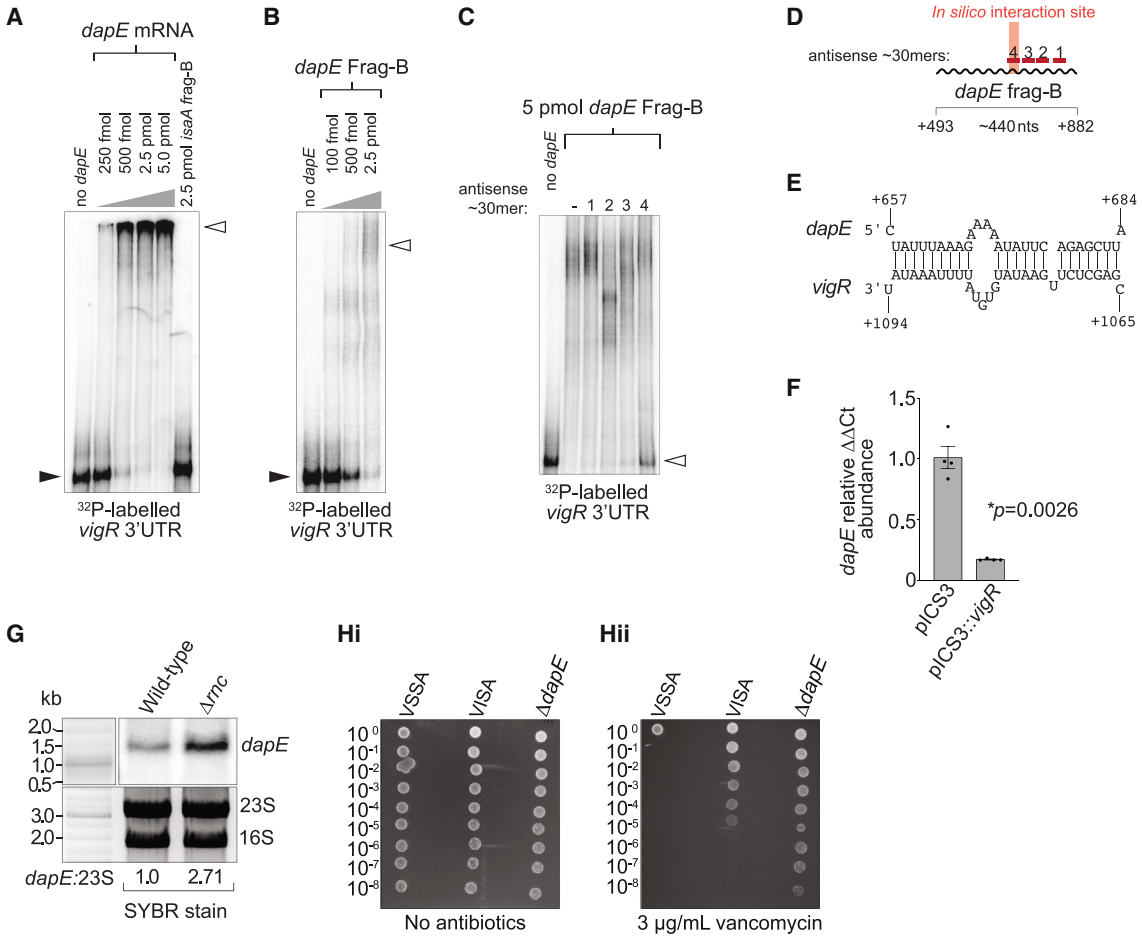

Figure 4. The succinyl-diaminopimelate desuccinylase *dapE* is regulated by *vigR* 3′ UTR

(A) EMSA analysis of the RNA-RNA interaction between *vigR* 3′ UTR and *dapE* mRNA. A total of 50 fM of radiolabeled *vigR* 3′ UTR (bottom) was titrated against increasing concentrations of the *dapE* mRNA (top). The *isaA* fragment B (Frag-B) RNA was titrated against 50 fM of radiolabeled *vigR* 3′ UTR as a known negative control.[14]

(B) The *dapE* mRNA was synthesized as sub-fragments (~400 nt in length) and used for EMSA analysis. *dapE* fragment B RNA and concentrations are indicated (top). Black arrowheads indicate migration of free, radiolabeled *vigR* 3′ UTR, and open arrowheads indicate slow migrating *vigR-dapE* duplexes.

(C) EMSA analysis of interactions between *vigR* 3′ UTR and *dapE* Frag-B (0 or 5 pmol). Antisense competitor oligonucleotides 1–4 (top) were spiked in at 500× excess concentration.

(D) The antisense oligonucleotide competitors 1–4 used for EMSA analysis are indicated relative to the *dapE* Frag-B RNA. The start and end positions of *dapE* Frag-B are indicated representative of the *dapE* transcription start site (+1 site). The predicted *in silico* interaction site is indicated in red (top).

(E) The predicted interaction seed between the *vigR-dapE* RNA species. The start and end positions of the RNA-RNA duplex are indicated representative of both mRNA transcription start sites.

(F) Histogram of RT-qPCR to quantify *dapE* chromosomal abundance (relative to *gapA*) in the JKD6009 pICS3 and pICS3*vigR* constructs. Error bars represent standard error of the mean (SEM). The Student's t test, two-sample assuming unequal variance was used to determine statistical significance, $p = 0.0026$, $n = 4$.

(G) Northern blot analysis of the *dapE* mRNA. Total RNA was extracted from *S. aureus* strain JKD6009 (isogenic parent) and Δ*rnc* grown in BHI to an OD_{578nm} of 3.0 and probed for *dapE* RNA. Sybr Green II-stained 23S and 16S rRNAs are indicated below as a loading control. Quantification of the ratio of 23S rRNA to *dapE* by densitometry is indicated below.

(H) Spotted dilution assays on solid Mueller-Hinton (MH) quantified vancomycin tolerance in *S. aureus* strains JKD6009 (VSSA), JKD6008 (VISA, isogenic parent), and Δ*dapE*. Culture dilution is indicated on left. The cultures were grown in the absence (i) or presence (ii) of 3 μg/mL vancomycin.

the *vigR-dapE* interaction may create an RNase III targeting site. Our data indicate that mRNA-mRNA interactions can have both activating and repressing regulatory outcomes in bacteria.

By intersecting RNA-seq and MAPS data, we have uncovered a functional interaction between *dapE* mRNA and the *vigR* 3′ UTR. DapE is a succinyl-diaminopimelate desuccinylase that is required for lysine and peptidoglycan synthesis.[37] Repression of *dapE* and activation of *isaA* expression (a cell wall autolysin) suggest that *vigR* upregulation coordinates a reduction in cell wall peptidoglycan crosslinking. Lysine is required for transpeptidation of peptidoglycan in *S. aureus*, and IsaA cleaves the glycosidic bonds between the MurNAc and GlcNAc sugars within peptidoglycan strands. This coordinated reduction

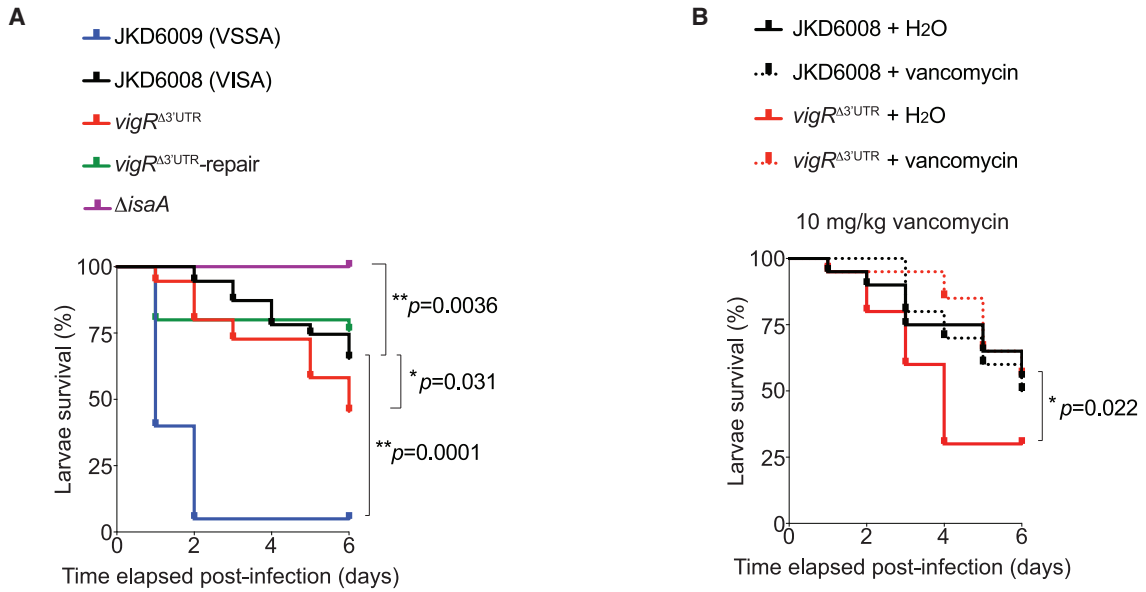

Figure 5. The *vigR* 3′ UTR and *isaA* mRNA are required for pathogenesis

(A) Kaplan-Meier survival plot of *G. mellonella* larvae infected with 10^7 CFU of *S. aureus* constructs (top) over the course of 6 days. Plots show an average of 4 independent replicates with 5 larvae per replicate ($n = 20$). Significant differences between survival curves were determined by log rank test at $^*p < 0.05$ and $^{**}p < 0.005$.

(B) The *vigR* 3′ UTR contributes to vancomycin tolerance during infection. Larvae were infected with 10^7 CFU of JKD6008 and $vigR^{\Delta 3'UTR}$ strains and challenged with either 10 mg/kg of vancomycin or H_2O over the course of 6 days. Plots show an average of 2 independent replicates with 10 larvae per replicate ($n = 20$). Significant differences between curves were determined by log rank test at $^*p < 0.05$.

in peptidoglycan crosslinking would be consistent with the reduced cell wall crosslinking, reduced autolysis, and vancomycin tolerance that is observed in VISA strains.[2]

Cell wall thickening and reduced crosslinking are thought to contribute to vancomycin tolerance in VISA; however, these strains are generally less virulent in wax moth and mouse models of infection.[35,36] We have confirmed this phenotype for VISA JKD6008 and found that upregulation of *vigR* in the VISA strain partially contributes to both vancomycin tolerance *in vivo* and to the reduced virulence phenotype. Deletion of the lytic transglycosylase *isaA* but not *dapE* completely attenuated virulence in the wax moth model. Previous studies have demonstrated that passive immunization with IsaA-targeting IgG[48] can reduce mortality in a mouse model of infection, indicating that IsaA is presented on the surface of the cell during infection, and our data suggest that IsaA may also contribute to virulence in VISA strain JKD6008, although the mechanism remains unclear. Cell wall metabolism appears to change during infections, and the ability to cleave peptidoglycan plays an important role in virulence.[49] The glucosaminidase SagB (that cleaves peptidoglycan) is required for virulence in mice, although the precise mechanism is also unknown.[49] The cell wall autolysin LytM is required for release of protein A in *S. aureus*, linking cell wall hydrolysis to virulence[50] and suggesting a potential mechanism for Δ*isaA* attenuation—through release of virulence factors at the cell surface.

Collectively, our data indicate that the long 3′ UTR of *vigR* has been functionalized by the acquisition of STAR sequence repeat insertions that encode conserved structured RNA. The JKD6008 genome encodes at least 101 STARs, and based on our earlier mapping of transcript boundaries,[14] we predict that 51 of these are transcribed. The *vigR* 3′ UTR facilitates interactions with both *dapE* and *isaA* mRNAs, which is predicted to reduce cell wall peptidoglycan crosslinking. The *vigR* 3′ UTR reduces virulence in a wax moth model of infection, consistent with the VISA phenotype—but this does not appear to be dependent on upregulation of *isaA* that is required for larvae killing. Our results support a broader role for *vigR* 3′ UTR in regulation of cell wall metabolism that contributes to both vancomycin tolerance and reduced virulence in VISA.

Limitations of the study

While the *G. mellonella* larvae serve as a well-established infection model for assessing *S. aureus* pathogenesis, additional research employing mice models and diverse clinical VISA isolates is essential to fully elucidate the potential therapeutic implications of targeting *vigR* and *isaA* mRNAs for RNA-based therapeutics. From a bacterial gene regulation perspective, further investigations are warranted to identify the specific conditions that induce *vigR* expression and the potential (if any) upstream involvement(s) of regulatory transcription factors in modulating *vigR* abundance within the cell. Such studies would significantly enhance our understanding of *S. aureus* cell wall biology and gene regulation. Moreover, exploring the functional implications of the spacer-STAR insertional elements across the entire *S. aureus* transcriptome, as well as in other clinical isolates, represents a critical avenue for future research aimed at deciphering

the intricate regulatory networks governing gene expression in *S. aureus*.

STAR★METHODS

Detailed methods are provided in the online version of this paper and include the following:

- KEY RESOURCES TABLE
- RESOURCE AVAILABILITY
  - Lead contact
  - Material availability
  - Data and code availability
- EXPERIMENTAL MODEL AND STUDY PARTICIPANT DETAILS
- METHOD DETAILS
  - Bacterial strains and general culture conditions
  - Strain modifications and plasmids
  - *vigR* conservation analysis
  - Northern blot
  - *In silico* RNA structure prediction
  - *In vitro* structure of *vigR* 3′ UTR
  - MS2-affinity purification and RNA-sequencing (MAPS)
  - Analysis of enriched nucleotide peak data
  - RNA-RNA electrophoretic mobility shift assay (EMSA)
  - Quantitative real-time PCR (qRT-PCR)
  - Vancomycin spot plate dilution assay
  - *Galleria mellonella* infection assay
- QUANTIFICATION AND STATISTICAL ANALYSIS

SUPPLEMENTAL INFORMATION

Supplemental information can be found online at https://doi.org/10.1016/j.celrep.2024.114082.

ACKNOWLEDGMENTS

The authors thank Ian Monk for insightful discussions of *S. aureus* phylogenetics. The authors acknowledge the use of facilities in the Structural Biology Facility within the Mark Wainwright Analytical Center, UNSW, funded in part by the Australian Research Council Linkage Infrastructure, Equipment and Facilities Grant (ARC LIEF, 190100165). D.G.M. and J.J.T. are supported by grants from the National Health and Medical Research Council (NHMRC, GNT1139313) and the Australian Research Council (ARC, DP220101938). This project received funding from the European Union's H2020 research and innovation programme under grant agreement no. 753137. This work of the Interdisciplinary Thematic Institute IMCBio, as part of the ITI 2021–2028 program of the University of Strasbourg, CNRS, and Inserm, was supported by IdEx Unistra (ANR-10-IDEX-0002) and by SFRI-STRAT'US project (ANR 20-SFRI-0012) and EUR IMCBio (ANR-17-EURE-0023) under the framework of the French Investments for the Future Program.

AUTHOR CONTRIBUTIONS

Conceptualization: D.G.M. and J.J.T.; investigation: D.G.M., W.D., D.L., H.D., A.P., K.N.R., K.A.M., T.P.S., A.K.C., and J.J.T.; methodology: D.G.M., W.D., D.L., H.D., A.P., K.N.R., A.K.C., and J.J.T.; supervision: D.G.M., A.K.C., and J.J.T.; writing – original draft preparation: D.G.M. and J.J.T.; writing – review and editing: D.G.M., W.D., D.L., H.D., A.P., K.N.R., K.A.M., T.P.S., A.K.C., and J.J.T.

DECLARATION OF INTERESTS

The authors declare no competing interests.

Received: May 22, 2023
Revised: January 17, 2024
Accepted: March 25, 2024
Published: April 6, 2024

REFERENCES

1. Tong, S.Y.C., Davis, J.S., Eichenberger, E., Holland, T.L., and Fowler, V.G., Jr. (2015). *Staphylococcus aureus* infections: epidemiology, pathophysiology, clinical manifestations, and management. Clin. Microbiol. Rev. *28*, 603–661. https://doi.org/10.1128/CMR.00134-14.
2. Howden, B.P., Davies, J.K., Johnson, P.D.R., Stinear, T.P., and Grayson, M.L. (2010). Reduced vancomycin susceptibility in *Staphylococcus aureus*, including vancomycin-intermediate and heterogeneous vancomycin-intermediate strains: resistance mechanisms, laboratory detection, and clinical implications. Clin. Microbiol. Rev. *23*, 99–139. https://doi.org/10.1128/CMR.00042-09.
3. Bandyra, K.J., Said, N., Pfeiffer, V., Górna, M.W., Vogel, J., and Luisi, B.F. (2012). The seed region of a small RNA drives the controlled destruction of the target mRNA by the endoribonuclease RNase E. Mol. Cell *47*, 943–953. https://doi.org/10.1016/j.molcel.2012.07.015.
4. Papenfort, K., Sun, Y., Miyakoshi, M., Vanderpool, C.K., and Vogel, J. (2013). Small RNA-mediated activation of sugar phosphatase mRNA regulates glucose homeostasis. Cell *153*, 426–437. https://doi.org/10.1016/j.cell.2013.03.003.
5. Bouvier, M., Sharma, C.M., Mika, F., Nierhaus, K.H., and Vogel, J. (2008). Small RNA binding to 5' mRNA coding region inhibits translational initiation. Mol. Cell *32*, 827–837. https://doi.org/10.1016/j.molcel.2008.10.027.
6. Jagodnik, J., Chiaruttini, C., and Guillier, M. (2017). Stem-loop structures within mRNA coding sequences activate translation initiation and mediate control by small regulatory RNAs. Mol. Cell *68*, 158–170.e3. https://doi.org/10.1016/j.molcel.2017.08.015.
7. Mediati, D.G., Wu, S., Wu, W., and Tree, J.J. (2021). Networks of resistance: Small RNA control of antibiotic resistance. Trends Genet. *37*, 35–45. https://doi.org/10.1016/j.tig.2020.08.016.
8. Durica-Mitic, S., Göpel, Y., and Görke, B. (2018). Carbohydrate utilization in bacteria: Making the most out of sugars with the help of small regulatory RNAs. Microbiol. Spectr. *6*. https://doi.org/10.1128/microbiolspec.RWR-0013-2017.
9. Sy, B.M., and Tree, J.J. (2020). Small RNA regulation of virulence in pathogenic *Escherichia coli*. Front. Cell. Infect. Microbiol. *10*, 622202. https://doi.org/10.3389/fcimb.2020.622202.
10. Chabelskaya, S., Gaillot, O., and Felden, B. (2010). A *Staphylococcus aureus* small RNA is required for bacterial virulence and regulates the expression of an immune-evasion molecule. PLoS Pathog. *6*, e1000927. https://doi.org/10.1371/journal.ppat.1000927.
11. Das, S., Lindemann, C., Young, B.C., Muller, J., Österreich, B., Ternette, N., Winkler, A.C., Paprotka, K., Reinhardt, R., Förstner, K.U., et al. (2016). Natural mutations in a *Staphylococcus aureus* virulence regulator attenuate cytotoxicity but permit bacteremia and abscess formation. Proc. Natl. Acad. Sci. USA *113*, E3101–E3110. https://doi.org/10.1073/pnas.1520255113.
12. Morrison, J.M., Miller, E.W., Benson, M.A., Alonzo, F., 3rd, Yoong, P., Torres, V.J., Hinrichs, S.H., and Dunman, P.M. (2012). Characterization of SSR42, a novel virulence factor regulatory RNA that contributes to the pathogenesis of a *Staphylococcus aureus* USA300 representative. J. Bacteriol. *194*, 2924–2938. https://doi.org/10.1128/JB.06708-11.
13. McKellar, S.W., Ivanova, I., Arede, P., Zapf, R.L., Mercier, N., Chu, L.C., Mediati, D.G., Pickering, A.C., Briaud, P., Foster, R.G., et al. (2022). RNase III CLASH in MRSA uncovers sRNA regulatory networks coupling

metabolism to toxin expression. Nat. Commun. *13*, 3560. https://doi.org/10.1038/s41467-022-31173-y.

14. Mediati, D.G., Wong, J.L., Gao, W., McKellar, S., Pang, C.N.I., Wu, S., Wu, W., Sy, B., Monk, I.R., Biazik, J.M., et al. (2022). RNase III-CLASH of multi--drug resistant *Staphylococcus aureus* reveals a regulatory mRNA 3' UTR required for intermediate vancomycin resistance. Nat. Commun. *13*, 3558. https://doi.org/10.1038/s41467-022-31177-8.
15. Mayr, C. (2017). Regulation by 3' untranslated regions. Annu. Rev. Genet. *51*, 171–194. https://doi.org/10.1146/annurev-genet-120116-024704.
16. Menendez-Gil, P., Caballero, C.J., Catalan-Moreno, A., Irurzun, N., Barrio-Hernandez, I., Caldelari, I., and Toledo-Arana, A. (2020). Differential evolution in 3' UTRs leads to specific gene expression in *Staphylococcus*. Nucleic Acids Res. *48*, 2544–2563. https://doi.org/10.1093/nar/gkaa047.
17. Cramton, S.E., Schnell, N.F., Götz, F., and Brückner, R. (2000). Identification of a new repetitive element in *Staphylococcus aureus*. Infect. Immun. *68*, 2344–2348. https://doi.org/10.1128/IAI.68.4.2344-2348.2000.
18. Purves, J., Blades, M., Arafat, Y., Malik, S.A., Bayliss, C.D., and Morrissey, J.A. (2012). Variation in the genomic locations and sequence conservation of STAR elements among *Staphylococcal* species provides insight into DNA repeat evolution. BMC Genom. *13*, 515. https://doi.org/10.1186/1471-2164-13-515.
19. Frith, M.C., Saunders, N.F.W., Kobe, B., and Bailey, T.L. (2008). Discovering sequence motifs with arbitrary insertions and deletions. PLoS Comput. Biol. *4*, e1000071. https://doi.org/10.1371/journal.pcbi.1000071.
20. Sassi, M., Augagneur, Y., Mauro, T., Ivain, L., Chabelskaya, S., Hallier, M., Sallou, O., and Felden, B. (2015). SRD: A *Staphylococcus* regulatory RNA database. RNA *21*, 1005–1017. https://doi.org/10.1261/rna.049346.114.
21. Yao, Z., Weinberg, Z., and Ruzzo, W.L. (2006). CMfinder – a covariance model based RNA motif finding algorithm. Bioinformatics *22*, 445–452. https://doi.org/10.1093/bioinformatics/btk008.
22. Rivas, E., Clements, J., and Eddy, S.R. (2020). Estimating the power of sequence covariation for detecting conserved RNA structure. Bioinformatics *36*, 3072–3076. https://doi.org/10.1093/bioinformatics/btaa080.
23. Weinberg, Z., and Breaker, R.R. (2011). R2R – software to speed the depiction of aesthetic consensus RNA secondary structures. BMC Bioinf. *12*, 3. https://doi.org/10.1186/1471-2105-12-3.
24. Baek, M., McHugh, R., Anishchenko, I., Jiang, H., Baker, D., and DiMaio, F. (2024). Accurate prediction of protein-nucleic acid complexes using RoseTTAFoldNA. Nat. Methods *21*, 117–121. https://doi.org/10.1038/s41592-023-02086-5.
25. Reuter, J.S., and Mathews, D.H. (2010). RNAstructure: Software for RNA secondary structure prediction and analysis. BMC Bioinf. *11*, 129. https://doi.org/10.1186/1471-2105-11-129.
26. Lalaouna, D., and Massé, E. (2015). Identification of sRNA interacting with a transcript of interest using MS2-affinity purification coupled with RNA sequencing (MAPS) technology. Genom. Data *5*, 136–138. https://doi.org/10.1016/j.gdata.2015.05.033.
27. Said, N., Rieder, R., Hurwitz, R., Deckert, J., Urlaub, H., and Vogel, J. (2009). *In vivo* expression and purification of aptamer-tagged small RNA regulators. Nucleic Acids Res. *37*, e133. https://doi.org/10.1093/nar/gkp719.
28. Helle, L., Kull, M., Mayer, S., Marincola, G., Zelder, M.E., Goerke, C., Wolz, C., and Bertram, R. (2011). Vectors for improved *Tet* repressor-dependent gradual gene induction or silencing in *Staphylococcus aureus*. Microbiology (Read.) *157*, 3314–3323. https://doi.org/10.1099/mic.0.052548-0.
29. Mercier, N., Prévost, K., Massé, E., Romby, P., Caldelari, I., and Lalaouna, D. (2021). MS2-affinity purification coupled with RNA sequencing in Gram-positive Bacteria. J. Vis. Exp. https://doi.org/10.3791/61731.
30. Langenberger, D., Bermudez-Santana, C., Hertel, J., Hoffmann, S., Khaitovich, P., and Stadler, P.F. (2009). Evidence for human microRNA-offset RNAs in small RNA sequencing data. Bioinformatics *25*, 2298–2301. https://doi.org/10.1093/bioinformatics/btp419.
31. Webb, S., Hector, R.D., Kudla, G., and Granneman, S. (2014). PAR-CLIP data indicate that Nrd1-Nab3-dependent transcription termination regulates expression of hundreds of protein-coding genes in yeast. Genome Biol. *15*, R8. https://doi.org/10.1186/gb-2014-15-1-r8.
32. Love, M.I., Huber, W., and Anders, S. (2014). Moderated estimation of fold change and dispersion for RNA-seq data with DESeq2. Genome Biol. *15*, 550. https://doi.org/10.1186/s13059-014-0550-8.
33. Ivain, L., Bordeau, V., Eyraud, A., Hallier, M., Dreano, S., Tattevin, P., Felden, B., and Chabelskaya, S. (2017). An *in vivo* reporter assay for sRNA-directed gene control in Gram-positive bacteria: Identifying a novel sRNA target in *Staphylococcus aureus*. Nucleic Acids Res. *45*, 4994–5007. https://doi.org/10.1093/nar/gkx190.
34. Born, T.L., and Blanchard, J.S. (1999). Structure/function studies on enzymes in the diaminopimelate pathway of bacterial cell wall biosynthesis. Curr. Opin. Chem. Biol. *3*, 607–613. https://doi.org/10.1016/s1367-5931(99)00016-2.
35. Cameron, D.R., Lin, Y.H., Trouillet-Assant, S., Tafani, V., Kostoulias, X., Mouhtouris, E., Skinner, N., Visvanathan, K., Baines, S.L., Howden, B., et al. (2017). Vancomycin-intermediate *Staphylococcus aureus* isolates are attenuated for virulence when compared with susceptible progenitors. Clin. Microbiol. Infect. *23*, 767–773. https://doi.org/10.1016/j.cmi.2017.03.027.
36. Jin, Y., Yu, X., Zhang, S., Kong, X., Chen, W., Luo, Q., Zheng, B., and Xiao, Y. (2020). Comparative analysis of virulence and toxin expression of vancomycin-intermediate and vancomycin-sensitive *Staphylococcus aureus* strains. Front. Microbiol. *11*, 596942. https://doi.org/10.3389/fmicb.2020.596942.
37. Gillner, D.M., Becker, D.P., and Holz, R.C. (2013). Lysine biosynthesis in bacteria: A metallodesuccinylase as a potential antimicrobial target. J. Biol. Inorg. Chem. *18*, 155–163. https://doi.org/10.1007/s00775-012-0965-1.
38. Chan, J.J., Tabatabaeian, H., and Tay, Y. (2023). 3' UTR heterogeneity and cancer progression. Trends Cell Biol. *33*, 568–582. https://doi.org/10.1016/j.tcb.2022.10.001.
39. De Gregorio, E., Abrescia, C., Carlomagno, M.S., and Di Nocera, P.P. (2002). The abundant class of nemis repeats provides RNA substrates for ribonuclease III in *Neisseriae*. Biochim. Biophys. Acta *1576*, 39–44. https://doi.org/10.1016/s0167-4781(02)00290-7.
40. De Gregorio, E., Silvestro, G., Petrillo, M., Carlomagno, M.S., and Di Nocera, P.P. (2005). Enterobacterial repetitive intergenic consensus sequence repeats in Yersiniae: Genomic organization and functional properties. J. Bacteriol. *187*, 7945–7954. https://doi.org/10.1128/JB.187.23.7945-7954.2005.
41. De Gregorio, E., Silvestro, G., Venditti, R., Carlomagno, M.S., and Di Nocera, P.P. (2006). Structural organization and functional properties of miniature DNA insertion sequences in Yersiniae. J. Bacteriol. *188*, 7876–7884. https://doi.org/10.1128/JB.00942-06.
42. Knutsen, E., Johnsborg, O., Quentin, Y., Claverys, J.P., and Håvarstein, L.S. (2006). BOX elements modulate gene expression in *Streptococcus pneumoniae*: Impact on the fine-tuning of competence development. J. Bacteriol. *188*, 8307–8312. https://doi.org/10.1128/JB.00850-06.
43. Maquat, L.E. (2020). Short interspersed nuclear element (SINE)-mediated post-transcriptional effects on human and mouse gene expression: SINE-UP for active duty. Philos. Trans. R. Soc. Lond. B Biol. Sci. *375*, 20190344. https://doi.org/10.1098/rstb.2019.0344.
44. Gong, C., and Maquat, L.E. (2011). lncRNAs transactivate STAU1-mediated mRNA decay by duplexing with 3' UTRs via Alu elements. Nature *470*, 284–288. https://doi.org/10.1038/nature09701.
45. Lucas, B.A., Lavi, E., Shiue, L., Cho, H., Katzman, S., Miyoshi, K., Siomi, M.C., Carmel, L., Ares, M., Jr., and Maquat, L.E. (2018). Evidence for convergent evolution of SINE-directed Staufen-mediated mRNA decay. Proc. Natl. Acad. Sci. USA *115*, 968–973. https://doi.org/10.1073/pnas.1715531115.

46. Ignatov, D., Vaitkevicius, K., Durand, S., Cahoon, L., Sandberg, S.S., Liu, X., Kallipolitis, B.H., Rydén, P., Freitag, N., Condon, C., and Johansson, J. (2020). An mRNA-mRNA interaction couples expression of a virulence factor and its chaperone in *Listeria monocytogenes*. Cell Rep. *30*, 4027–4040.e7. https://doi.org/10.1016/j.celrep.2020.03.006.

47. Liu, N., Niu, G., Xie, Z., Chen, Z., Itzek, A., Kreth, J., Gillaspy, A., Zeng, L., Burne, R., Qi, F., and Merritt, J. (2015). The *Streptococcus mutans irvA* gene encodes a trans-acting riboregulatory mRNA. Mol. Cell *57*, 179–190. https://doi.org/10.1016/j.molcel.2014.11.003.

48. Lorenz, U., Lorenz, B., Schmitter, T., Streker, K., Erck, C., Wehland, J., Nickel, J., Zimmermann, B., and Ohlsen, K. (2011). Functional antibodies targeting IsaA of *Staphylococcus aureus* augment host immune response and open new perspectives for antibacterial therapy. Antimicrob. Agents Chemother. *55*, 165–173. https://doi.org/10.1128/AAC.01144-10.

49. Sutton, J.A.F., Carnell, O.T., Lafage, L., Gray, J., Biboy, J., Gibson, J.F., Pollitt, E.J.G., Tazoll, S.C., Turnbull, W., Hajdamowicz, N.H., et al. (2021). *Staphylococcus aureus* cell wall structure and dynamics during host-pathogen interaction. PLoS Pathog. *17*, e1009468. https://doi.org/10.1371/journal.ppat.1009468.

50. Becker, S., Frankel, M.B., Schneewind, O., and Missiakas, D. (2014). Release of protein A from the cell wall of *Staphylococcus aureus*. Proc. Natl. Acad. Sci. USA *111*, 1574–1579. https://doi.org/10.1073/pnas.1317181111.

51. Taylor, R.G., Walker, D.C., and McInnes, R.R. (1993). *E. coli* host strains significantly affect the quality of small scale plasmid DNA preparations used for sequencing. Nucleic Acids Res. *21*, 1677–1678. https://doi.org/10.1093/nar/21.7.1677.

52. Monk, I.R., Tree, J.J., Howden, B.P., Stinear, T.P., and Foster, T.J. (2015). Complete bypass of restriction systems for major *Staphylococcus aureus* lineages. mBio *6*, e00308–e315. https://doi.org/10.1128/mBio.00308-15.

53. Howden, B.P., Seemann, T., Harrison, P.F., McEvoy, C.R., Stanton, J.A.L., Rand, C.J., Mason, C.W., Jensen, S.O., Firth, N., Davies, J.K., et al. (2010). Complete genome sequence of *Staphylococcus aureus* strain JKD6008, an ST239 clone of methicillin-resistant *Staphylococcus aureus* with intermediate-level vancomycin resistance. J. Bacteriol. *192*, 5848–5849. https://doi.org/10.1128/JB.00951-10.

54. Kuroda, M., Kuroda, H., Oshima, T., Takeuchi, F., Mori, H., and Hiramatsu, K. (2003). Two-component system VraSR positively modulates the regulation of cell-wall biosynthesis pathway in *Staphylococcus aureus*. Mol. Microbiol. *49*, 807–821. https://doi.org/10.1046/j.1365-2958.2003.03599.x.

55. Carrel, M., Perencevich, E.N., and David, M.Z. (2015). USA300 methicillin-resistant *Staphylococcus aureus*, United States, 2000-2013. Emerg. Infect. Dis. *21*, 1973–1980. https://doi.org/10.3201/eid2111.150452.

56. Nair, D., Memmi, G., Hernandez, D., Bard, J., Beaume, M., Gill, S., Francois, P., and Cheung, A.L. (2011). Whole-genome sequencing of *Staphylococcus aureus* strain RN4220, a key laboratory strain used in virulence research, identifies mutations that affect not only virulence factors but also the fitness of the strain. J. Bacteriol. *193*, 2332–2335. https://doi.org/10.1128/JB.00027-11.

57. Frei, A., King, A.P., Lowe, G.J., Cain, A.K., Short, F.L., Dinh, H., Elliott, A.G., Zuegg, J., Wilson, J.J., and Blaskovich, M.A.T. (2021). Nontoxic cobalt(III) Schiff base complexes with broad-spectrum antifungal activity. Chemistry *27*, 2021–2029. https://doi.org/10.1002/chem.202003545.

58. Anders, S., Pyl, P.T., and Huber, W. (2015). HTSeq – A Python framework to work with high-throughput sequencing data. Bioinformatics *31*, 166–169. https://doi.org/10.1093/bioinformatics/btu638.

59. Sullivan, M.J., Petty, N.K., and Beatson, S.A. (2011). Easyfig: A genome comparison visualizer. Bioinformatics *27*, 1009–1010. https://doi.org/10.1093/bioinformatics/btr039.

60. Schindelin, J., Arganda-Carreras, I., Frise, E., Kaynig, V., Longair, M., Pietzsch, T., Preibisch, S., Rueden, C., Saalfeld, S., Schmid, B., et al. (2012). Fiji: An open-source platform for biological-image analysis. Nat. Methods *9*, 676–682. https://doi.org/10.1038/nmeth.2019.

61. Sy, B., Wong, J., Granneman, S., Tollervey, D., Gally, D., and Tree, J.J. (2018). High-resolution, high-throughput analysis of Hfq-binding sites using UV crosslinking and analysis of cDNA (CRAC). Methods Mol. Biol. *1737*, 251–272. https://doi.org/10.1007/978-1-4939-7634-8_15.

62. Holmqvist, E., Wright, P.R., Li, L., Bischler, T., Barquist, L., Reinhardt, R., Backofen, R., and Vogel, J. (2016). Global RNA recognition patterns of post-transcriptional regulators Hfq and CsrA revealed by UV crosslinking *in vivo*. EMBO J. *35*, 991–1011. https://doi.org/10.15252/embj.201593360.

63. Tsai, C.J.Y., Loh, J.M.S., and Proft, T. (2016). *Galleria mellonella* infection models for the study of bacterial diseases and for antimicrobial drug testing. Virulence *7*, 214–229. https://doi.org/10.1080/21505594.2015.1135289.

STAR★METHODS

KEY RESOURCES TABLE

REAGENT or RESOURCE	SOURCE	IDENTIFIER
Bacterial and virus strains		
Escherichia coli K-12 strain DH5α	Taylor et al.[51]	DH5α
Escherichia coli K-12 strain IMO8B	Monk et al.[52]	IM08B
Staphylococcus aureus subsp. *aureus* (ST239) JKD6008	Howden et al.[53]	JKD6008
Staphylococcus aureus subsp. *aureus* (ST239) JKD6009	Howden et al.[53]	JKD6009
Staphylococcus aureus subsp. *aureus* (ST239) JKD6008 *vigR*$^{\Delta 3'UTR}$	Mediati et al.[14]	JKD6008 *vigR*$^{\Delta 3'UTR}$
Staphylococcus aureus subsp. *aureus* (ST239) JKD6008 *vigR*$^{\Delta 3'UTR}$-repair	Mediati et al.[14]	JKD6008 *vigR*$^{\Delta 3'UTR}$-repair
Staphylococcus aureus subsp. *aureus* (ST239) JKD6008 Δ*isaA*	Mediati et al.[14]	JKD6008 Δ*isaA*
Staphylococcus aureus subsp. *aureus* (ST239) JKD6008 Δ*dapE*	This study	JKD6008 Δ*dapE*
Staphylococcus aureus subsp. *aureus* (ST239) JKD6004	Howden et al.[2]	JKD6004
Staphylococcus aureus subsp. *aureus* (ST5) Mu50	Kuroda et al.[54]	Mu50
Staphylococcus aureus subsp. *aureus* (ST8) USA300 (NRS384)	Carrel et al.[55]	USA300
Staphylococcus aureus subsp. *aureus* RN4220	Nair et al.[56]	RN4220
Chemicals, peptides, and recombinant proteins		
GlycoBlue	Invitrogen	Cat#AM9516
Lead(II) acetate	Sigma-Aldrich	Cat#32307
Benzoyl cyanide	Sigma-Aldrich	Cat#115959
Vancomycin hydrochloride	Sigma-Aldrich	Cat#1404939
Anhydrotetracycline hydrochloride	Sigma-Aldrich	Cat#37919-100MG-R
Chloramphenicol	Sigma-Aldrich	Cat#C0378
Ampicillin sodium salt	Sigma-Aldrich	Cat#69523
γ^{32}P-ATP	PerkinElmer	Cat#BLU502A250UC
Amylose resin	New England Biolabs	Cat#E8021S
SYBR safe DNA stain	ThermoFisher	Cat#2687599
SYBR Green II RNA stain	ThermoFisher	Cat#S7564
ULTRAhyb buffer	ThermoFisher	Cat#AM8669
Dimethyl sulfoxide	Sigma-Aldrich	Cat#D2650-5X5ML
Ammonium persulfate	Sigma-Aldrich	Cat#A3678
cOmplete mini EDTA-free protease inhibitor tablets	Roche	Cat#4693159001
X-gal solution	Invitrogen	Cat#R0941
Phenol solution	Sigma-Aldrich	Cat#P4557-400mL
Acrylamide/Bis-acrylamide 40% solution	Sigma-Aldrich	Cat#A9926
Glyoxal solution	Sigma-Aldrich	Cat#50649-25mL
T4 DNA ligase	ThermoFisher	Cat#15224017
T4 polynucleotide kinase	New England Biolabs	Cat#M0201S
DNase I	New England Biolabs	Cat#M0303S
Calf intestinal alkaline phosphatase	Promega	Cat#M2825
RQ1 RNase-free DNase	Promega	Cat#M6101
RNasIN ribonuclease inhibitor recombinant	Promega	Cat#N2511
Critical commercial assays		
Wizard SV gel and PCR clean-up system	Promega	Cat#A9282
Wizard genomic DNA purification kit	Promega	Cat#A1120
Wizard plus SV miniprep DNA purification system	Promega	Cat#A1460

(*Continued on next page*)

Continued

REAGENT or RESOURCE	SOURCE	IDENTIFIER
HiScribe T7 quick high-yield RNA synthesis kit	New England Biolabs	Cat#E2050S
Phusion hot-start flex 2x master mix	New England Biolabs	Cat#M0536S
SuperScript IV first-strand system	ThermoFisher	Cat#18091050
NEBNext II directional RNA library kit	New England Biolabs	Cat#E7760S
SensiFAST SYBR Hi-ROX kit	Bioline	Cat#BIO-92005
Deposited data		
MAPS sequencing data	NCBI GEO	GSE252940
Experimental models: Organisms/strains		
Galleria mellonella wax moth	Frei et al.[57]	*G. mellonella*
Oligonucleotides		
As per Table S5	This study	N/A
Recombinant DNA		
As per Table S5	This study	N/A
Software and algorithms		
GraphPad Prism	Version 10.1.1	https://www.graphpad.com
CRAC_pipeline_SE.py	Webb et al.[31]	https://git.ecdf.ed.ac.uk/sgrannem/crac_pipelines
pyCRAC	Webb et al.[31]	https://git.ecdf.ed.ac.uk/sgrannem/pycrac
Blockbuster	Langenberger et al.[30]	https://www.bioinf.unileipzig.de/~david/LIFE/LIFE/blockbuster.html
HTSeq	Anders et al.[58]	N/A
DEseq2	Love et al.[32]	N/A
GLAM2	Frith et al.[19]	https://meme-suite.org/meme/tools/glam2
GLAM2SCAN	Frith et al.[19]	https://meme-suite.org/meme/tools/glam2scan
CMfinder	Yao et al.[21]	N/A
R-scape	Rivas et al.[22]	http://eddylab.org/R-scape/
R2R	Weinberg & Breaker[23]	http://breaker.research.yale.edu/R2R
RoseTTAFold2NA	Baek et al.[24]	https://github.com/uw-ipd/RoseTTAFold2NA
RNAstructure	Reuter and Mathews[25]	http://rna.urmc.rochester.edu/RNAstructure.html
Other		
Microspin G-50 column	Cytiva	Cat#GE27-5330-01
Bio-Rad disposable bio-spin column	Bio-Rad	Cat#7326204

RESOURCE AVAILABILITY

Lead contact

Further information and requests for resources and reagents should be directed to and will be fulfilled by the lead contact, Jai J. Tree (j.tree@unsw.edu.au).

Material availability

Material generated in this study will be made available in request following publication.

Data and code availability

- MAPS sequencing data generated in this publication are available at NCBI Gene Expression Omnibus (GEO) under the accession GSE252940 (https://www.ncbi.nlm.nih.gov/geo/query/acc.cgi?acc=GSE252940).
- This study did not generate original code.
- Any additional information required to reanalyze the data reported in this paper is available from the lead contact upon request.

EXPERIMENTAL MODEL AND STUDY PARTICIPANT DETAILS

The *Galleria mellonella* colony was originally obtained from Westmead Hospital (Sydney, NSW Australia) and have been continuously maintained at Macquarie University (Sydney, NSW Australia) since 2019. Larvae were reared in controlled environmental chambers at 30°C and 65% humidity with a 12-h light/dark cycle. *G. mellonella* larvae are widely used as a replacement model for toxicity and efficacy testing and as invertebrates, are exempt from ethical approval.

METHOD DETAILS

Bacterial strains and general culture conditions

The bacterial strains, plasmids and oligonucleotides used in this study are listed in Table S5. *S. aureus* strains JKD6004,[2] Mu50,[54] USA300,[55] RN4220[56] and the JKD6009/JKD6008 (VSSA/VISA) pair[53] were routinely cultured at 37°C on solid or in liquid brain heart infusion (BHI, Merck) or Mueller-Hinton (MH, Merck) media. Antibiotics were used in this study to select for plasmids in *S. aureus* at 15 μg/mL chloramphenicol, unless otherwise specified. *E. coli* DH5α[51] and IM08B[52] were cultured at 37°C on solid or in liquid Luria-Bertani (LB) media. Antibiotics were used to select for plasmids in *E. coli* at 100 μg/mL ampicillin or 15 μg/mL chloramphenicol, unless otherwise specified. All bacterial strains were stored at −80°C as stationary phase cultures with 16% (v/v) glycerol.

Strain modifications and plasmids

S. aureus MS2-affinity tagged constructs were constructed in the ATc inducible $P_{xyl/tet}$ pRAB11 vector.[28] The *vigR* 3′ UTR sequence was amplified from JKD6009 using Phusion Hot Start Polymerase (NEB) with primers incorporating the MS2 aptamer sequence (fused to the 5′ end of *vigR* 3′ UTR) and the *rrn1* T7 terminator (Table S5). The MS2-*vigR* 3′ UTR and MS2 products were cloned into pRAB11 at the KpnI/EcoRI sites using 10 U of T4 DNA ligase (Thermo) and transformed into chemically-competent *E. coli* DH5α. Constructs were confirmed by Sanger sequencing, transformed into electrocompetent *E. coli* IM08B and then transformed into electrocompetent *S. aureus* JKD6009 $vigR^{\Delta 3'UTR}$.

The JKD6008 Δ*dapE* strain was constructed using the pIMAY-Z vector and allelic exchange.[52] At least 500-nt flanking regions using primer pairs detailed in Table S5 were amplified from JKD6008 and annealed together using splicing by overlap extension (SOE) PCR. The mutant was passaged and selected on solid BHI and confirmed using allele-specific PCR (Table S5). Loss of the pIMAY-Z vector was confirmed by chloramphenicol sensitivity and plasmid-specific PCR (Table S5). Construction of the JKD6009 $vigR^{\Delta 3'UTR}$, JKD6009 pICS3*vigR,* JKD6008 $vigR^{\Delta 3'UTR}$, JKD6008 $vigR^{\Delta 3'UTR}$-repair and JKD6008 Δ*isaA* strains were described previously in Mediati et al.[14] The pICS3*vigR*-STARless vector was constructed by amplifying flanking regions of the JKD6009 *vigR* 3′ UTR sequence (Δ+866–955 nt) using primer pairs detailed in Table S5 and annealed together using SOE PCR. The purified PCR product was cloned into the pICS3-P_{tufA} vector[14] using the PstI/EcoRI sites and confirmed using Sanger sequencing.

vigR conservation analysis

The mRNA transcriptional boundary of *vigR* in *S. aureus* strain JKD6009 was determined from our previous work using dRNA-seq, Term-seq and Northern blot.[14] These boundary nucleotides were used to define and extract the *vigR* mRNA sequence from 58 genomes of *S. aureus* isolates. The 5′ UTR, CDS and 3′ UTR sequence length, number of STARs, and presence or absence of the *folD* or *isaA* mRNA interaction seed region in each isolate were determined individually and used to construct Table S1. From these 58 *S. aureus* genomes, 14 representative strains were selected that demonstrated *vigR* transcript variation. The GenBank and blastn.out files from these 14 representative strains were used as input into Easyfig[59] to generate Figure 1A.

Northern blot

At least 5 μg of RNA was treated with a 5:1 ratio of glyoxal denaturation mixture for 1 h at 55°C. Denatured RNA was resolved on a 1% BPTE-agarose gel containing SYBR Green (Thermo) and run for ∼1 h at 100 V in 1x BPTE buffer. Intact 23S and 16S ribosomal RNA was confirmed on a Bio-Rad Chemi-doc and washed consecutively in 200 mL of 75 mM NaOH, 200 mL of neutralizing solution (1.5 M NaCl and 500 mM Tris-HCl, pH 7.5) and 200 mL of SSC buffer (3 M NaCl and 300 mM sodium citrate, pH 7.0) for 20 min each. RNA was capillary transferred onto a Hybond-N+ nylon membrane (GE Healthcare) and UV-crosslinked in a Stratagene auto-crosslinker with 1200 mJ dosage of UV-C. The membrane was equilibrated in ULTRAhyb buffer (Thermo) for 1 h at 42°C and then incubated with 10 pMol of 20 μCi γ^{32}P-ATP-labelled oligonucleotide probe (Table S5) for 16 h at 42°C. Membranes were washed three times in 2x sodium chloride sodium phosphate EDTA (SSPE) buffer with the addition of 0.1% SDS for 20 min at 42°C. The blot was imaged using a BAS-MP 2040 phosphorscreen on a FLA9500 Typhoon (GE Healthcare). ImageJ[60] was used to align the SYBR stained gel and membrane, and used to construct Figure 1B.

In silico RNA structure prediction

The STAR sequence repeats, as defined previously by Purves et al.[18] (5' – TNTGTTGNGGCCCN), and the upstream 50 nt within JKD60008 were extrapolated and used as input into the GLAM2 software[19] to generate the consensus Spacer-STAR sequence motif in Figure 2A. GLAM2 was used with the gapless Gibbs sampling parameter and accommodates short sequence gaps. This consensus Spacer-STAR motif was inserted into GLAM2SCAN[19] and used to identify related sequences within the JKD6008

genome. The transcriptional boundaries as identified previously using dRNA-seq and Term-seq[14] were then used to determine the genomic features (e.g., UTR, CDS or ncRNA) that each Spacer-STAR sequence is positioned in. These 101 Spacer-STAR sequences defined by GLAM2SCAN were then used as input into CMfinder[21] and used to construct the *in silico* consensus RNA secondary structure model in Figure 2B using the covariance model expectation maximisation algorithm. The R-scape software[22] was used to assess statistical significance of the co-varying base pairs. The computational prediction of the Spacer-STAR RNA structures in Figure 2C were performed using the deep-learning biomolecular prediction software RoseTTAFold2NA (RF2NA)[24] (https://github.com/uw-ipd/RoseTTAFold2NA). RF2NA version 0.2 was used for all structure prediction calculations (ID: 03f12bd421db618455d9c0726f79f72433a8638e) with a community submitted code patch applied to handle unexpected letters in the multiple sequence alignment stage (pull request #59 in RF2NA GitHub repository). Computational predictions were performed on an Ubuntu 22.04 Linux server equipped with a single A100 NVIDIA GPU boasting 40 GB of random-access memory. Specific software configurations included NVIDIA driver v535.86.10 and CUDA version 12.2. Databases used for RF2NA analyses included model weights from April 2023, structure templates from March 2021, and the Uniref. 30 database from February 2023. The versions of Rfam, BFD, and RNACentral databases and annotations were current as of August 2023. The nucleotide sequences of the *vigR* spacer-STARs within *S. aureus* isolate JKD6008 are presented in Table S6.

In vitro structure of *vigR* 3′ UTR

Purified *vigR* 3′ UTR amplified from JKD6008 was *in vitro* transcribed using HiScribe T7 RNA polymerase (NEB). RNA products were DNase I treated (NEB) for 30 min at 37°C, phenol-chloroform extracted, ethanol precipitated, and then separated on a 4% polyacrylamide TBE-6M urea gel. Products were excised, crushed, and incubated in 500 μL gel elution buffer (10 mM magnesium acetate, 500 mM ammonium acetate, 1 mM EDTA) with gentle rotation for 16 h at 4°C. RNA was extracted from the eluate using phenol-chloroform and ethanol precipitated. Approx. 5 pMol of purified *vigR* 3′ UTR RNA was renatured by heating to 90°C for 2 min, placed on ice for 2 min, and then incubated in folding buffer (300 mM HEPES (pH 8.0), 20 mM $MgCl_2$ and 300 mM NaCl) for 1 h at 37°C. RNA was then chemically modified with 10, 50 and 100 mM of benzoyl cyanide (Sigma) for 1 min at 20°C. RNA species were also modified with 10 mM lead acetate (Sigma) for 1 min at 25°C. As a no-modification control, DMSO (Sigma) was added to the RNA and incubated for 1 min at 20°C. RNA species were ethanol precipitated and reverse-transcribed using SuperScript IV (Thermo) with purified 30 μCi ^{32}P-ATP-labeled oligonucleotides spanning the entire *vigR* 3′ UTR (Figure S2B; and Table S5). In parallel, single ddNTP (Roche) sequencing reactions were performed with identical 30 μCi ^{32}P-ATP-labeled oligonucleotides and 2 pMol of RNA. The cDNA products were incubated with 200 mM NaOH at 80°C to hydrolyze template RNA and inactivate SuperScript IV enzyme. Products were separated on a 6% polyacrylamide TBE-6M urea gel for 100 min at a maximum of 50 W (Figure S2B). Gels were then dried and visualised using a Fuji BAS-MP 2040 phosphorscreen and Typhoon FLA9500. Nucleotide reactivity was analyzed and RNAstructure[25] was used to construct the secondary structure model in Figure 2D.

MS2-affinity purification and RNA-sequencing (MAPS)

JKD6009 *vigR*$^{\Delta 3'UTR}$ transformed with pRAB11MS2-*vigR* 3′UTR and pRAB11MS2 (MS2 tag only control) were grown in BHI supplemented with 15 μg/mL chloramphenicol at 37°C with 180 rpm shaking to an OD_{600nm} 3.0. Constructs were then induced with 0.4 μM ATc and grown for a further 15 min at 37°C with shaking. Cultures were harvested by centrifugation at 4°C and crude extracts (5 μg) were probed for the MS2 aptamer sequence. MS2-affinity purifications were performed in biological duplicates and as previously described.[26,29] RNA quality was assessed on a PicoRNA Bioanalyzer 2100 chip and underwent ribosomal RNA depletion using QIAseq FastSelect (Qiagen). Sequencing libraries were constructed using the NEBNext II directional RNA library kit for Illumina sequencing (NEB) and sequenced on a NextSeq2000 platform at the Epitranscriptomics and RNA-sequencing facility, Université de Lorraine-CNRS-INSERM (Nancy, France) generating 50 bp single-end reads.

Analysis of enriched nucleotide peak data

MAPS data were analyzed using the ruffus pipeline CRAC_pipeline_PE.py previously described for CRAC data analysis[61] that performs alignment and read counting steps (https://git.ecdf.ed.ac.uk/sgrannem/crac_pipelines). Binding sites were identified using blockbuster[61] and adapted from Holmqvist et al.[62] The GTF format outputs from the ruffus CRAC pipeline were converted to BED format using pyGTF2bed.py.[31] The experimental replicates were combined and sorted before peak calling. Peaks were defined using blockbuster with settings: -minBlockHeight 50 -distance 1. Peak intervals defined by blockbuster were used to calculate statistically enriched regions of the transcriptome. Read depth at peak intervals was calculated for each experimental and control replicate using HTSeq,[58] and enriched peaks identified using DESeq2.[32]

RNA-RNA electrophoretic mobility shift assay (EMSA)

Full-length or sub-fragments of *dapE* (SAA6008_RS11085), *spn* (SAA6008_RS02260), *hysA* (SAA6008_RS12255) and *vigR* 3′ UTR from JKD6008 were *in vitro* transcribed using HiScribe T7 RNA polymerase (NEB). RNA products were RQ1 DNase treated (Promega) for 15 min at 37°C, phenol-chloroform extracted and ethanol precipitated, and then separated on a 5% polyacrylamide TBE-6M urea gel. Products were excised, crushed, and incubated in 500 μL RNA gel elution buffer (10 mM magnesium acetate, 500 mM ammonium acetate, 1 mM EDTA) for 16 h at 4°C. RNA was extracted from the eluate using phenol-chloroform extraction and ethanol precipitation. Approximately 50 pMol of *vigR* 3′ UTR RNA was dephosphorylated using quick calf intestinal alkaline phosphatase (CIP,

Thermo), then extracted using phenol-chlorofom and ethanol precipitation. The 5′ ends were radiolabeled with 20 μCi γ^{32}P-ATP using T4 polynucleotide kinase (NEB) and separated from free nucleotides using a MicroSpin G-50 column (Cytiva), and then purified on denaturing PAGE as above. To analyze *vigR* 3′ UTR binding to full-length or sub-fragments of *dapE* (Figure S4B), increasing excess amounts of the *dapE* RNAs were annealed to 50 fM of radiolabeled *vigR* 3′ UTR in 1x duplex buffer (40 mM Tris-acetate, 0.5 mM magnesium acetate, 100 mM NaCl) in a 10 μL reaction. These were incubated at 95°C for 5 min, then at 37°C for 2 h. Samples were run on a 4% polyacrylamide 0.5X TBE gel containing 5% glycerol for ~4 h at a maximum of 16V/cm or 1.33 mA/cm. Gels were then dried and visualised using a Fuji BAS-MP 2040 phosphorscreen and Typhoon FLA9500. Where appropriate 1.25 μM of antisense competitor oligonucleotides (Table S5) were added to compete away radiolabeled *vigR* 3′ UTR at a concentration excess of 500x. RNA was annealed, run and visualised as above.

Quantitative real-time PCR (qRT-PCR)

JKD6009 pICS3 or pICS3*vigR*[14] overnight cultures were diluted 1/100 into 10 mL BHI and grown at 37°C with 200 rpm shaking to OD_{600nm} 3.0. Cells were harvested by spinning at 3,800 *g* for 10 min at 4°C. A total of 5 U of recombinant RNasIN (Promega) and 10 U of RQ1 RNase-free DNase (Promega) was added and RNA purified using the GTC-phenol:chloroform extraction procedure for *S. aureus*.[14] At least 1 μg of RNA was reverse-transcribed using SuperScript IV (Thermo). qRT-PCR was performed on a RotorGene Q (Eppendorf) using the SensiFAST SYBR Hi-ROX kit (Bioline). A total cDNA concentration of 100 ng in combination with 200 nM of *dapE* oligonucleotide per reaction (Table S5) resulted in ideal Ct values of between 8 and 12. The Ct values per reaction were calculated using the RotorGene Q analysis software (Qiagen). Relative gene expression was determined using ΔΔCt abundance of the *gapA* (SAA6008_RS08745, glyceraldehyde-3-phosphate dehydrogenase) transcript as a reference control.

Vancomycin spot plate dilution assay

JKD6008, JKD6008 Δ*dapE*, JKD6009 and JKD6009 containing pICS3 constructs (Table S5) were used to inoculate 5 mL of liquid MH, supplemented with 10 μg/mL chloramphenicol where appropriate and grown for 16 h at 37°C with 200 rpm shaking. Cultures were aliquoted into a 96-well microtitre plate, serially diluted (up to 10^{-8}) into fresh liquid MH and spotted onto solid MH plates supplemented with and without vancomycin (2–3 μg/mL). Spot plates were air dried at room temperature and incubated for 24 h at 37°C. Plates were imaged on a Bio-Rad Chemi-doc using the *trans*-white light settings.

Galleria mellonella infection assay

G. mellonella larvae (230–250 mg) were injected with 10^7 bacterial cells of each *S. aureus* construct (JKD6009, JKD6008 (isogenic parent), $vigR^{\Delta 3'UTR}$, $vigR^{\Delta 3'UTR}$-repair and Δ*isaA*) and a PBS control into the last right proleg using a 100 μL syringe (Hamilton Ltd).[57] The PBS-injected larvae resulted in no killing. The assay was done with 4 replicates using 5 larvae per replicate (n = 20). Following infection, the larvae were incubated at 37°C for 6 consecutive days and monitored every 24 h for health and survival according to the *G. mellonella* Health Index Scoring System.[63] To examine vancomycin tolerance in JKD6009, JKD6008, $vigR^{\Delta 3'UTR}$ and Δ*dapE* strains, larvae (230–250 mg) were infected with 10^7 bacterial cells and incubated at 37°C for 1 h. Either vancomycin (10 mg/kg) or distilled water was injected into the infected larvae and treated as above. The assay was performed with 2 replicates using 10 larvae per treatment for each replicate (n = 20).

QUANTIFICATION AND STATISTICAL ANALYSIS

General statistical analyses were performed using GraphPad Prism v10.1.1. The statistical test used to determine significance is indicated in the figure legends and where appropriate the statistical threshold used is also indicated.